

## NUMERICAL APPROXIMATION OF NORMALLY HYPERBOLIC INVARIANT MANIFOLDS

HENK BROER<sup>1</sup> AARON HAGEN<sup>2</sup> AND GERT VEGTER<sup>1</sup>

<sup>1</sup>Department of Mathematics and Computing Science  
University of Groningen, The Netherlands

<sup>2</sup>Department of Mathematics  
University of Texas at Arlington, TX 76019

**Abstract.** This paper deals with the numerical continuation of invariant manifolds, regardless of the restricted dynamics. Typically, invariant manifolds make up the skeleton of the dynamics of phase space. Examples include limit sets, co-dimension 1 manifolds separating basins of attraction (separatrices), stable/unstable/center manifolds, nested hierarchies of attracting manifolds in dissipative systems and manifolds in phase plus parameter space on which bifurcations occur. These manifolds are for the most part invisible to current numerical methods. The approach is based on the general principle of normal hyperbolicity, where the graph transform leads to the numerical algorithms. This gives a highly multiple purpose method. The key issue is the discretization of the differential geometric components of the graph transform, and its consequences. Examples of computations will be given, with and without non-uniform adaptive refinement.

**1. Introduction.** Invariant manifolds of dynamical systems largely determine the geometry of their phase space. Codimension 1 manifolds, for example, may separate several basins of attraction. But in general equilibria, closed curves, invariant tori, their stable and unstable manifolds etc. are the corner stones around which a more detailed analysis may be in order. If the invariant manifold of interest, say  $\Sigma_1$ , is not an attractor, it may still lie in a higher dimensional invariant manifold,  $\Sigma_2$ , which is. If the dynamics are restricted to  $\Sigma_2$  then  $\Sigma_1$  may even serve as a separatrix. This is the kind of situation we want to look at in the present paper. To fix thoughts think of  $\Sigma_2$  being a 3–torus attractor with phase lock dynamics, where the aim is to visualize an unstable 2–torus  $\Sigma_1$  inside this 3–torus.

The key notion needed here is *normal hyperbolicity* of the invariant manifold. Normal hyperbolicity is a necessary and sufficient condition for the smooth persistence of the manifold under small perturbations of the system. This condition states that the normal to the manifold splits into stable (contractive) and unstable (expansive) subspaces. Also, it is required that the contraction tangent to the manifold is dominated by the contraction normal to the manifold [8, 11].

The persistence of normally hyperbolic manifolds enables us to develop *robust* numerical algorithms that compute these manifolds by numerical continuation. At each step of the continuation process we use the *graph transform* to find the new ‘perturbed’ invariant manifold. The graph transform is a classical tool for proving the invariant manifold theorem (see Section 2). This transform is a contraction on a Banach space of functions, whose graph is near the invariant manifold. The fixed point of the graph transform corresponds to the invariant manifold itself [8, 11].

---

1991 *Mathematics Subject Classification.* 34C28, 34C30, 34C45, 37D10, 37M99, 65D18, 65P99.

*Key words and phrases.* Invariant manifolds, normal hyperbolicity, chaotic dynamics, numerical continuation, bifurcation theory, computational geometry, graph transform.

Simple iteration of a dynamical system has been used a lot in the literature to visualize invariant manifolds. However, in general it is impossible to numerically locate an invariant manifold by iteration, even in the case of a normally hyperbolic attractor. The reason is that the manifold may contain smaller attractors, like in the case of  $\Sigma_2$ . Our method is independent of the dynamics on the manifold and can in principal be used to compute  $\Sigma_2$ .

Another advantage of our method can be explained by the example of  $\Sigma_2$ . Now finding the separatrix 2-torus  $\Sigma_1$  within  $\Sigma_2$  is hardly possible by simple iteration. Indeed, the numerical errors grow exponentially in the unstable direction. However, since  $\Sigma_1$  in the ambient space is normally hyperbolic of saddle-type, our methods apply. In fact, our approach will reverse this numerical instability, effectively making  $\Sigma_1$  a stable object. We emphasize that the algorithm converges whether the dynamics on  $\Sigma_1$  is quasi-periodic or more complicated, regardless.

The computation of invariant manifolds of higher dimension has been addressed in the literature previously. Dieci and Lorenz [6] developed a method to compute hyperbolic attracting tori. They use the graph transform and global parametrizations of the tori. See also, for example, [7] and [14]. Broer, Osinga, and Vegter [4] present a method to compute saddle-type manifolds. They use the graph transform and simplicial complexes to approximate manifolds. See also [9]. In the present paper, a method of approximating smooth manifolds by discrete objects is given. Starting with a simplicial complex, our approximation is piecewise polynomial. To do this, a discrete tubular neighborhood [10] is constructed. The approach here approximates the manifold locally using polynomial maps from the tangent space to the normal space. A non-uniform approximation of arbitrary order for any manifold is obtained. This is applied to a numerical implementation of the graph transform. See also [1], which focuses on the convergence and contractivity of the graph transform algorithm. One example in the present paper is a new approach to computing the so-called “slow transient” surface in chemical kinetics [15]. There is currently no general way to compute these surfaces.

**2. The graph transform and invariant manifold theorem.** This section reviews part of the theory of normally hyperbolic manifolds and paves the way for the development of an efficient algorithm for their computation. A formulation of a classical method of proving the Invariant Manifold Theorem is given (the graph transform) from which the algorithm is derived.

Consider a  $C^r$  diffeomorphism  $F$  on  $\mathbb{R}^n$ , having an  $r$ -normally hyperbolic invariant manifold  $\Sigma \subset \mathbb{R}^n$ . By the *Invariant Manifold Theorem* [11, Theorem 4.1], a  $C^r$  diffeomorphism  $\tilde{F}$ , that is  $C^r$ -near  $F$ , has a locally unique  $r$ -normally hyperbolic invariant manifold  $\tilde{\Sigma}$ , that is  $C^r$  and  $C^r$ -near  $\Sigma$ . Our goal is the computation of  $\tilde{\Sigma}$ .

Given any vector bundle  $N(\Sigma)$  transverse to  $T(\Sigma)$ , there is an induced *hyperbolic splitting*  $N^u(\Sigma) \oplus T(\Sigma) \oplus N^s(\Sigma)$ , where  $N(\Sigma) = N^u(\Sigma) \oplus N^s(\Sigma)$ . Here,  $N^s(\Sigma)$  is the *stable bundle* and  $N^u(\Sigma)$  is the *unstable bundle*. In computations, the choice made for  $N(\Sigma)$  is the bundle orthogonal to  $T(\Sigma)$ , with respect to the Euclidean norm. This choice has several advantages, indicated in [1]. However, in this paper, by the notation  $N(\Sigma)$  we mean any bundle transverse to  $T(\Sigma)$ .

The perturbed manifold  $\tilde{\Sigma}$  is computed using a continuation algorithm. One step of the algorithm has two parts. The initial data is an  $F$ -invariant manifold  $\Sigma$  with its hyperbolic splitting  $N^u(\Sigma) \oplus T(\Sigma) \oplus N^s(\Sigma)$ . The first step uses the graph transform on  $\Sigma$  with  $N^u(\Sigma) \oplus T(\Sigma) \oplus N^s(\Sigma)$  to determine the  $\tilde{F}$ -invariant manifold  $\tilde{\Sigma}$ . The second step uses the *linear graph transform*  $\mathcal{L}$  together with initial data determined by  $\tilde{\Sigma}$  and  $N^u(\Sigma) \oplus T(\Sigma) \oplus N^s(\Sigma)$  to determine the hyperbolic splitting

$N^u(\tilde{\Sigma}) \oplus T(\tilde{\Sigma}) \oplus N^s(\tilde{\Sigma})$  of  $\tilde{\Sigma}$ . Now the first and second steps may be repeated with initial data  $\tilde{\Sigma}$  and  $N^u(\tilde{\Sigma}) \oplus T(\tilde{\Sigma}) \oplus N^s(\tilde{\Sigma})$ . For the formulation of  $\mathcal{L}$ , see [3].

To formulate the graph transform, it is assumed that  $N_y^s(\Sigma)$  (resp.  $N_y^u(\Sigma)$ ),  $y \in \Sigma$ , are Lipschitz continuous functions  $\Sigma \rightarrow \mathcal{G}_{n,j}$ . Here,  $\mathcal{G}_{n,j}$  is the Grassmann manifold of  $j$ -planes of  $\mathbb{R}^n$ , where  $j = \dim N^s(\Sigma)$  (resp.  $N^u(\Sigma)$ ). Under these assumptions,  $N(\Sigma) = N^u(\Sigma) \oplus N^s(\Sigma)$  induces a tubular neighborhood  $U$  of  $\Sigma$ , [10]. In fact,  $U$  is lipeomorphic (homeomorphic by a Lipschitz map with Lipschitz inverse) to  $\{(p, v) : p \in \Sigma, v \in N_p(\Sigma), |v| < \epsilon\}$  for some  $\epsilon > 0$ . The point  $(p, v) \in N(\Sigma)$  corresponds to the point  $p + v \in U$ . From now on we take  $N(\Sigma) = \{(p, v) : p \in \Sigma, v \in N_p(\Sigma), |v| < \epsilon\}$ , and do not distinguish between  $N(\Sigma)$  and the neighborhood  $U$  of  $\Sigma$ .

We look for an  $\tilde{F}$ -invariant manifold  $\tilde{\Sigma}$  in the neighborhood  $U$  of  $\Sigma$ . Now,  $\tilde{\Sigma}$  will be represented as a graph in  $N^s(\Sigma)$  plus a graph in  $N^u(\Sigma)$ . Thus, suppose that  $\mathcal{S}_{\epsilon, \delta}^s$  is the space of Lipschitz sections of  $N^s(\Sigma)$  with Lipschitz constant less than  $\delta$ , [8, 11], where  $\epsilon$  is the diameter of the tubular neighborhood  $U$ . Similarly define  $\mathcal{S}_{\epsilon, \delta}^u$ . Elements of  $\mathcal{S}_{\epsilon, \delta}^s$  are Lipschitz maps  $\sigma^s : \Sigma \rightarrow N^s(\Sigma)$ , and we write  $\sigma^s(p) = (p, v^s(p))$ , for some  $v^s(p) \in N_p^s(\Sigma)$ . The notation for  $\mathcal{S}_{\epsilon, \delta}^u$  is analogous. The space  $\mathcal{S}_{\epsilon, \delta}^s$  ( $\mathcal{S}_{\epsilon, \delta}^u$ ) with the natural  $C^0$  norm on sections, denoted  $|\cdot|_b$ , is complete. Now define  $\mathcal{S}_{\epsilon, \delta}$  to be the set of all pairs of sections  $(\sigma^s, \sigma^u)$  with  $\sigma^s \in \mathcal{S}_{\epsilon, \delta}^s$  and  $\sigma^u \in \mathcal{S}_{\epsilon, \delta}^u$ . The space  $\mathcal{S}_{\epsilon, \delta}$  is complete with respect to the norm  $\|(\sigma^s, \sigma^u)\| \equiv \max\{|\sigma^s|_b, |\sigma^u|_b\}$ . If  $\sigma = (\sigma^s, \sigma^u) \in \mathcal{S}_{\epsilon, \delta}$ ,  $\sigma^s(p) = (p, v^s(p))$  and  $\sigma^u(p) = (p, v^u(p))$ , then

$$\text{graph}\{\sigma\} \equiv \{p + v^s(p) + v^u(p) : p \in \Sigma\}$$

is a Lipschitz manifold near  $\Sigma$  in Lipschitz norm for small  $\epsilon, \delta$ .

The graph transform  $\Gamma : \mathcal{S}_{\epsilon, \delta} \rightarrow \mathcal{S}_{\epsilon, \delta}$  in this setting is formulated in [1]. It may be described concisely in geometrical terms. In the attracting case, given  $\sigma$ ,  $\Gamma(\sigma)$  is characterized by the property that the graph of  $\Gamma(\sigma)$  equals the  $\tilde{F}$ -image of the graph of  $\sigma$ . The repelling case is similar, with  $\tilde{F}$  replaced by  $\tilde{F}^{-1}$ . In the saddle case, one restricts attention to the stable and unstable bundles separately. The section  $\sigma \in \mathcal{S}_{\epsilon, \delta}$  is a fixed point of  $\Gamma$  if and only if the graph of  $\sigma$  is an  $\tilde{F}$ -invariant manifold. Furthermore, for  $\epsilon, \delta$ , and  $\|F - \tilde{F}\|_{C^1}$  small,  $\Gamma$  is a contraction [8, 11].

**3. Numerical discretization of graph transform.** In Section 2 we saw that  $\Gamma$  is characterized by its effect on the graphs of functions in  $\mathcal{S}_{\epsilon, \delta}$ . In fact, a numerical implementation of  $\Gamma$  is largely a matter of appropriately discretizing these *candidate manifolds*. For the implementation of  $\mathcal{L}$ , see [3].

In this section, we present a method for approximating the candidate manifolds by discrete elements, suitable for computer implementation. For this approximation scheme, as for the graph transform in Section 2, initial data consisting of a  $C^r$  compact manifold  $\Sigma \subset \mathbb{R}^n$ ,  $r \geq 1$ , with a Lipschitz transverse bundle  $N(\Sigma) = N^s(\Sigma) \oplus N^u(\Sigma)$  are required. A candidate manifold  $\tilde{\Sigma}$  is the sum of graphs of sections  $\sigma^s$  of  $N^s(\Sigma)$  and  $\sigma^u$  of  $N^u(\Sigma)$ . We approximate  $\tilde{\Sigma}$  using discrete sections of discrete vector bundles over a discrete manifold. The discrete manifold is a polyhedron approximating  $\Sigma$  and the discrete sections are polynomial over each face of the polyhedron, in appropriate coordinates. These coordinates are induced by the discrete vector bundles, which give a tubular neighborhood of  $\Sigma$ .

To be more specific, choose a simplicial complex  $\mathcal{C}$  whose vertices are contained in  $\Sigma$  and whose polyhedron is homeomorphic to  $\Sigma$ . Thus,  $\mathcal{C}$  is a *supporting* simplicial complex. Denote the polyhedron of  $\mathcal{C}$  by  $\Sigma_H^P$ , where  $H$  is the maximal diameter of the simplices of  $\mathcal{C}$ .

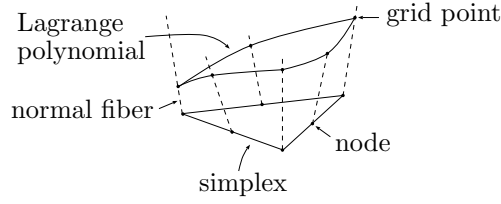
FIGURE 1. Discrete approximation to  $\tilde{\Sigma}$ ,  $p = 2$ , attracting caseThe fattened Thom map,  $\epsilon = 0.6$ ;  
 $p = 1$  adaptively refinedThe fattened 'sink' map,  $\epsilon = 0.4$ ;  
 $p = 1$ 

FIGURE 2. Invariant tori losing smoothness

The polynomials that make up the discrete sections are the Lagrange polynomials of order  $p \geq 1$  on a simplex. Say  $\dim \Sigma \equiv d \geq 1$ , and denote the  $d$ -simplices of  $\mathcal{C}$  by  $\mathcal{C}_1, \dots, \mathcal{C}_m$ . The Lagrange polynomials require data on the *principal lattice of order  $p$*  of each  $\mathcal{C}_k$ , [5]. The points of the lattice are called the 'nodes' of  $\mathcal{C}_k$ . For the interpolation to be well-behaved, the family of sets  $\{\mathcal{C}_i\}_{i=1}^m$ , with the associated parameter  $H$ , must be a *regular family* [5]. Roughly, this means none of the  $\mathcal{C}_i$  are almost contained in a  $(d-1)$ -dimensional hyperplane, uniformly as  $H \rightarrow 0$ .

To reduce the problem of interpolating points in a neighborhood of  $\Sigma$  to one involving interpolating points in Euclidean space, a (discrete) tubular neighborhood of  $\Sigma$  is required. We have that  $\Sigma_H^P$  is Lipschitz and  $\Sigma_H^P$  converges to  $\Sigma$  in Lipschitz norm as  $H \rightarrow 0$ . A tubular neighborhood of  $\Sigma$  will be induced by a (discrete) Lipschitz vector bundle  $N(\Sigma_H^P)$  over  $\Sigma_H^P$ , transverse to  $T(\Sigma)$ . We construct  $N(\Sigma_H^P)$  by interpolating the fibers of  $N(\Sigma)$  at the vertices of  $\Sigma_H^P$ , for small  $H$ . In fact, the approximation  $\tilde{\Sigma}_D$  to  $\tilde{\Sigma}$  will be the sum of graphs of sections of (discrete) stable and unstable bundles,  $N^s(\Sigma_H^P)$  and  $N^u(\Sigma_H^P)$ . On each  $\mathcal{C}_k$ ,  $N^s(\Sigma_H^P)$  (resp.  $N^u(\Sigma_H^P)$ ) is obtained by interpolating the fibers of  $N^s(\Sigma)$  (resp.  $N^u(\Sigma)$ ) at the vertices.

These interpolants will be functions  $\mathcal{C}_k \rightarrow \mathcal{G}_{n,j}$ , where  $j = \dim N^s(\Sigma)$  (resp.  $N^u(\Sigma)$ ) [18]. To interpolate the fibers, we use a local parametrization  $\phi$  of  $\mathcal{G}_{n,j}$ . The map  $\phi$  is constructed from  $n \times n$  *plane rotation matrices* (also called *Givens* or *Jacobi transformations*)  $G_i(\theta_i)$ ,  $i = 1, \dots, q \equiv j(n-j)$ . Suppose  $e_1, \dots, e_n \in \mathbb{R}^n$  are the standard basis vectors. Here,  $G_1$  is rotation in the plane span  $\{e_1, e_{n-j+1}\}$ ,  $G_2$  in plane span  $\{e_1, e_{n-j}\}$ ,  $\dots$ ,  $G_{n-j}$  in plane span  $\{e_1, e_2\}$ ,  $G_{n-j+1}$  in plane span  $\{e_2, e_{n-j+2}\}$ ,  $\dots$ ,  $G_{2(n-j)}$  in plane span  $\{e_2, e_3\}$ ,  $\dots$ ,  $G_{(j-1)(n-j)+1}$  in plane span  $\{e_j, e_n\}$ ,  $\dots$ ,  $G_{j(n-j)}$  in plane span  $\{e_j, e_{j+1}\}$ . For example, given a 1-plane  $U \in \mathcal{G}_{3,1}$ , we have  $U = \text{Range}\{G_1(\rho_1)G_2(\rho_2)e_1\}$  for some  $\rho_1, \rho_2 \in [0, \pi)$ . A local parametrization of  $\mathcal{G}_{3,1}$  near  $U$  is  $\phi(\theta_1, \theta_2) = \text{Range}\{G_1(\rho_1)G_2(\rho_2)G_1(\theta_1)G_2(\theta_2)e_1\}$ ,  $\theta_1, \theta_2 \in (-\epsilon, \epsilon)$ . Using  $\phi$ , fibers may be interpolated over  $\mathcal{C}_k$  by interpolating points in  $\mathbb{R}^q$  over  $\mathcal{C}_k$ . The interpolants  $\mathcal{C}_k \rightarrow \mathbb{R}^q$  are first order Lagrange polynomials.

Since  $N^s(\Sigma)$  and  $N^u(\Sigma)$  are Lipschitz, and  $\langle N_x^s(\Sigma), N_x^u(\Sigma) \rangle \geq \alpha > 0$  for  $x \in \Sigma$ , we may put  $N(\Sigma_H^P) \equiv N^s(\Sigma_H^P) \oplus N^u(\Sigma_H^P)$  for small  $H$ . The bundle  $N(\Sigma_H^P)$  is transverse to both  $\Sigma$  and  $\Sigma_H^P$  uniformly for  $H \rightarrow 0$ . In fact we have the stronger

condition that  $\{\langle \text{span}\{v_1\}, \text{span}\{v_2\} \rangle \geq \alpha > 0$ ,  $v_1 \in N_y(\Sigma_H^P)$ ,  $v_2 \in \text{span}\{\mathcal{C}_i\}$ , uniformly for  $y \in \Sigma_H^P$ , all  $\mathcal{C}_i \in \mathcal{C}$  containing  $y$ , and  $H \rightarrow 0$ . In addition,  $N(\Sigma_H^P)$  is Lipschitz, uniformly in  $H \rightarrow 0$ . To be precise, if, for any  $x \in \Sigma_H^P$ ,  $S_x \subset N_x(\Sigma_H^P) \subset \mathbb{R}^n$  is the unit  $(n-d)$ -sphere, then for some  $L > 0$ ,  $\text{dist}\{S_x, S_y\} \leq L|x-y|$ ,  $x, y \in \Sigma_H^P$ , uniformly for  $H \rightarrow 0$ . Hence,  $N(\Sigma_H^P)$  induces a tubular neighborhood  $U$  of  $\Sigma_H^P \subset \mathbb{R}^n$ , which contains  $\Sigma$  for small  $H$ .

Now, suppose the columns of the matrix  $E_k^s(x)$  form a smooth orthonormal basis for  $N_x^s(\Sigma_H^P)$ ,  $x \in \mathcal{C}_k$ . Similarly define  $E_k^u(x)$  for  $x \in \mathcal{C}_k$ . In terms of the bases for  $N_{\mathcal{C}_k}^s(\Sigma_H^P)$  and  $N_{\mathcal{C}_k}^u(\Sigma_H^P)$ , the discrete sections are given by Lagrange polynomials  $p_k^s : \mathcal{C}_k \rightarrow \mathbb{R}^j$ ,  $j = \dim N^s(\Sigma)$ , and  $p_k^u : \mathcal{C}_k \rightarrow \mathbb{R}^j$ ,  $j = \dim N^u(\Sigma)$ . The data at a node  $y \in \Sigma_H^P$  used to determine  $p_k^s$  ( $p_k^u$ ) is obtained as follows. Since  $\tilde{\Sigma}$  is Lipschitz-near  $\Sigma$ ,  $y + N_y(\Sigma_H^P)$  intersects  $\tilde{\Sigma}$  transversally, say at  $v \in N_y(\Sigma_H^P)$ . (The points  $y+v$  are called the ‘grid points’ of the discrete manifold.) Decompose  $v = v^s + v^u$ , where  $v^s \in N_y^s(\Sigma_H^P)$  and  $v^u \in N_y^u(\Sigma_H^P)$ . Then, the data for  $p_k^s$  ( $p_k^u$ ) are the coordinates of  $v^s$  ( $v^u$ ) in terms of the basis given by the columns of  $E_k^s(y)$  ( $E_k^u(y)$ ).

The discrete approximation to  $\tilde{\Sigma}$  is then the  $C^0$  manifold

$$\tilde{\Sigma}_D = \{y + E_k^s(y)p_k^s(y) + E_k^u(y)p_k^u(y) : y \in \mathcal{C}_k, k = 1, \dots, m\}.$$

See Figure 1. In fact,  $\text{dist}(\tilde{\Sigma}_D, \tilde{\Sigma}) = O(H^{p+1})$ , as  $H \rightarrow 0$ , provided  $\tilde{\Sigma}$  is of smoothness class  $C^{p+1}$ .

Now, for example in the attracting case, one iterate of the discrete graph transform  $\Gamma_D$  is characterized as follows. Given a discrete section  $\sigma_D$  of  $N(\Sigma_H^P)$ ,  $\Gamma_D(\sigma_D)$  is a discrete section with graph equal to the discrete approximation to the  $\tilde{F}$ -image of the graph of  $\sigma_D$ . Note that the performance of the algorithm depends on two separate numerical processes. The first is the iteration of  $\Gamma_D$ , which converges to, say,  $\tilde{\Sigma}_D$ , and the second is the convergence of  $\tilde{\Sigma}_D$  to the perturbed invariant manifold  $\tilde{\Sigma}$  as  $H \rightarrow 0$ , [1].

**4. Computations.** This section contains some of the numerical experiments done to test the algorithm outlined in Section 3. To demonstrate that the algorithm converges regardless of the dynamics on the manifold, examples were chosen with a wide variety of dynamics. No special difficulty was observed in the continuation due to these different dynamical scenarios. In Examples 1 and 2, continuation is carried out past the point where normal hyperbolicity of the torus is lost [1]. Also, in Examples 3 and 5, initial data is obtained by simulation, and is quite rough. Here,  $\Gamma_D$  converged with this rough initial data, smoothing it out. Examples 1 and 4 illustrate that  $\Gamma_D$  remains contractive for different values of  $p \geq 1$  and a non-uniform mesh. Additionally, in Examples 1 and 4, we were able to carry continuation farther than previously [4] due to the choice of the hyperbolic splitting [1]. Example 6 illustrates an extension to the case of computing just part of an invariant manifold. This is accomplished by local extrapolation of the manifold at the boundary after each continuation step. This approach makes no special requirement on the vector field on the boundary of the computed manifold. At different points along the boundary, the vector field may point outward, inward, be tangent to the boundary, etc.

**Example 1:** The 3D fattened Thom map [4]

$$\begin{aligned} x_{i+1} &= 0.1x_i + \epsilon \sin z_i \\ y_{i+1} &= z_i + y_i + \epsilon x_i \\ z_{i+1} &= 2z_i + y_i + \epsilon x_i \end{aligned} \quad , \quad (x_i, y_i, z_i) \in \mathbb{R} \times \mathbf{S}^1 \times \mathbf{S}^1 \quad (1)$$

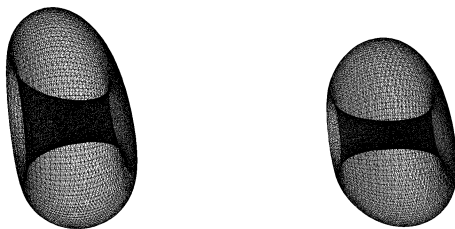
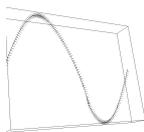
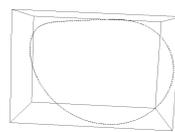


FIGURE 3. Lorenz-84 invariant tori; 32768 elements,  
 $p = 1$ ; left:  $F = 1.84$ , right:  $F = 1.755$



Arnold family curve,  $\epsilon = 0.78$ ;  
 50 elements,  $p = 3$



Lorenz system curve,  $r = 16.5$ ;  
 200 elements,  $p = 1$

FIGURE 4. Saddle-type invariant curves

For (1) with  $\epsilon = 0$ ,  $x = 0$  is an attracting torus with hyperbolic mixing. The torus loses hyperbolicity at  $\epsilon = 0.47$ . There appears to be a ridge along which the torus is losing smoothness. In fact, there is small scale bumpiness along the ridge of the torus in Figure 2, and this area is the site of a further loss of smoothness for increasing  $\epsilon$ . A computation of the same surface with  $p = 3$  is in [1].

**Example 2:** A fattened ‘sink’ map

$$\begin{aligned} x_{i+1} &= 0.25x_i + \epsilon \sin z_i \\ y_{i+1} &= y_i + 0.5 \sin y_i + \epsilon x_i \\ z_{i+1} &= z_i - 0.5 \cos y_i \sin z_i + \epsilon x_i \end{aligned}, \quad (x_i, y_i, z_i) \in \mathbb{R} \times \mathbf{S}^1 \times \mathbf{S}^1 \quad (2)$$

For (2) with  $\epsilon = 0$ ,  $x = 0$  is an attracting torus with a sink, source, and two saddles. At  $\epsilon = 0.13$ , the torus loses hyperbolicity at a sink. For  $\epsilon > 0.13$ , the sink has two stable complex conjugate eigenvalues whose eigenspace is a plane normal to the torus. See Figure 2.

**Example 3:** The ‘Lorenz-84’ system [16]

$$\begin{aligned} \dot{x} &= -y^2 - z^2 - 0.25x + 0.25F \\ \dot{y} &= xy - 4xy - y + G \\ \dot{z} &= 4xy + xz - z \end{aligned}, \quad (x, y, z) \in \mathbb{R}^3 \quad (3)$$

Example 3 is a truncation of a model of atmospheric circulation. System (3) exhibits a Hopf saddle–node bifurcation near  $(F, G) = (1.68, 1.68)$ , generating an invariant torus [12]. The torus was continued along a segment with  $G$  fixed, in both directions starting from  $(F, G) = (1.8, 1.65)$ . For  $F = 1.84$  and  $F = 1.755$ , computational instability was observed, although the torus apparently continues to exist. See Figure 3. This instability may be due to insufficient numerical resolution and weak attraction. Note for decreasing  $F$  the torus approaches a more sphere–like surface and the inner radius gets smaller. This is expected since the parameters approach the Hopf saddle–node point.

**Example 4:** The 3D-fattened Arnold family [4]

$$\begin{aligned} x_{i+1} &= x_i + 0.1 + \epsilon(y_i + z_i/2 + \sin x_i) \\ y_{i+1} &= 0.3(y_i + \sin x_i) \\ z_{i+1} &= 2.4(y_i + z_i + \sin x_i) \end{aligned}, \quad (x_i, y_i, z_i) \in \mathbf{S}^1 \times \mathbb{R}^2 \quad (4)$$



FIGURE 5. Enzyme reaction surface; left: 1024 elements,  $p = 1$ , right: 16384 elements,  $p = 1$

For  $\epsilon = 0$ , (4) has a closed curve of saddle-type. For increasing  $\epsilon$ , the curve is quasiperiodic with phase locking, then a saddle-node bifurcation occurs. We continued the curve to  $\epsilon = 0.78$ , near where the curve loses hyperbolicity. The last  $\epsilon$  value for which the hyperbolic splitting was computed was 0.6. In Figure 4, the angle between the stable and unstable parts of the hyperbolic splitting is small. Similar results were obtained in [4], where the curve was continued to  $\epsilon = 0.7125$ .

**Example 5:** The Lorenz system [17]

$$\begin{aligned} \dot{x} &= 10(y - x) \\ \dot{y} &= rx - y - xz, \quad (x, y, z) \in \mathbb{R}^3 \\ \dot{z} &= xy - (8/3)z \end{aligned} \quad (5)$$

At  $r = 20.0$ , (5) has a saddle-type periodic orbit, which was continued to  $r = 16.5$ . Figure 4 shows the final curve near a homoclinic orbit.

**Example 6:** An enzyme reaction [15]

$$\begin{aligned} \dot{s} &= -(1 - c - q)s + c \\ \dot{c} &= (1 - c - q)s - 2c + q, \quad (s, c, q) \in \mathbb{R}^3 \\ \dot{q} &= c - 1.1q \end{aligned} \quad (6)$$

In (6), the variables  $s$ ,  $c$ , and  $q$  are the concentrations of different chemical species undergoing chemical reaction. The flow is described by a nested hierarchy of attracting manifolds: a surface containing a curve, which contains an equilibrium. The part of the attracting surface in the region  $0 \leq c \leq 1$ ,  $0 \leq q \leq 1$ ,  $0 \leq s \leq 2$  was computed. This computation may be compared with the one in [15]. It may be possible to interactively determine the rate constants of chemical reactions using computations like this, by matching the surface to experimental data.

**5. Conclusion.** This paper was concerned with a general purpose approach to the computation of a normally hyperbolic invariant manifold. Here we address some practical numerical issues which arose during computations. To simplify the discussion, the attracting case is considered.

The main step of the algorithm approximates the point of intersection of a fiber of  $N(\Sigma_H^P)$  with the  $\tilde{F}$ -image of  $\tilde{\Sigma}_D$ . If  $\Sigma_H^P$  or the data from which  $N(\Sigma_H^P)$  is interpolated is not sufficiently smooth, the  $\tilde{F}$ -image of  $\tilde{\Sigma}_D$  may not intersect a fiber of  $N(\Sigma_H^P)$ . Also, when  $H$  becomes small compared to  $\epsilon$ , small irregularities in the data can become significant by causing the normal fibers to cross within a distance  $\epsilon$  along the fibers. To address these difficulties, a smoothing technique using local averaging was used, so that nearby normal fibers are more nearly parallel. For example, this was critical for the Lorenz-84 torus.

Another difficulty occurs if  $\Sigma$  has a sharp bend. In this case, the normal fibers near the bend spread out like a fan. Thus, the computed grid points on  $\tilde{\Sigma}_D$  may be much farther apart than the corresponding nodes on  $\Sigma_H^P$ . In this case, it is necessary to subdivide the  $d$ -simplices of  $\Sigma_H^P$  near the bend. For example, this occurred for the Lorenz system periodic orbit. This is a common issue in such computations.

For vector fields, computations are often work-intensive. First, having a reasonable number of  $d$ -simplices in  $\Sigma_H^P$  can exhaust memory, especially in higher

dimensions. In the Lorenz-84 example, the implementation of  $N(\Sigma_H^P)$  required memory near computer limits on an HP-9000-C200. Non-uniform approximation is important for this reason. Second, the vector field must be integrated. Thus, computations of manifolds with weak hyperbolicity, which require more iterates of  $\Gamma_D$ , can be lengthy.

**Acknowledgement.** The figures were generated using Geomview, developed at The Geometry Center at the University of Minnesota. The authors would like to thank Luca Dieci, Bernd Krauskopf, Hinke Osinga, Volker Reichelt, Carles Simo and Floris Takens for valuable discussions. This research was supported by the Netherlands Organisation for Scientific Research (NWO), project nr. 613-02-201, at the University of Groningen. See <http://home.nethere.net/hagen/>.

#### REFERENCES

- [1] H. W. Broer, A. Hagen and G. Vegter, *Multiple Purpose Algorithms for Invariant Manifolds*, Dynam. Contin. Discrete Implus. Systems B 10 (2003), 331–344.
- [2] H. W. Broer, A. Hagen and G. Vegter, *Finite element algorithms for invariant manifolds*, in preparation.
- [3] H. W. Broer, A. Hagen and G. Vegter, *Finite element algorithms for invariant manifolds—the saddle case*, in preparation.
- [4] H. W. Broer, H. M. Osinga and G. Vegter, *Algorithms for computing normally hyperbolic invariant manifolds*, Z. angew. Math. Phys. 48 (1997), 480–524.
- [5] P. G. Ciarlet and P.-A. Raviart, *General Lagrange and Hermite interpolation in  $\mathbb{R}^n$  with applications to finite element methods*, Arch. Rational Mech. Anal. 46 (1972), 177–199.
- [6] L. Dieci and J. Lorenz, *Computation of invariant tori by the method of characteristics*, SIAM J. Numer. Anal. 32 (1995), 1436–1474.
- [7] K. Edoh, R. Russel and W. Sun *Computation of invariant tori by orthogonal collocation*, Appl. Numer. Math. 32 (2000), 273–289.
- [8] N. Fenichel, *Persistence and smoothness of invariant manifolds for flows*, Indiana Univ. Math. J. 21 (1971/1972), 193–226.
- [9] H. Osinga, “Computing Invariant Manifolds,” Ph.D. Thesis, University of Groningen, The Netherlands, 1996.
- [10] M. W. Hirsch, “Differential Topology,” Springer-Verlag, New York, 1994.
- [11] M. W. Hirsch, C. C. Pugh and M. Shub, “Invariant Manifolds,” Springer-Verlag, New York, 1977.
- [12] Y. Kuznetsov, “Elements of applied bifurcation theory,” Springer-Verlag, New York, 1998.
- [13] J. Palis and F. Takens, “Hyperbolicity & sensitive chaotic dynamics at homoclinic bifurcations,” Cambridge University Press, Cambridge, 1993.
- [14] V. Reichelt, *Computing invariant tori and circles in dynamical systems*, IMA Vol. Math. Appl. 119 (2000), 407–437.
- [15] M. R. Roussel and S. J. Fraser, *On the geometry of transient relaxation*, J. Chem. Phys. 94 (1991), 7106–7113.
- [16] A. Shil’nikov, G. Nicolis, and C. Nicolis, *Bifurcation and predictability analysis of a low-order atmospheric circulation model*, Internat. J. Bifur. Chaos Appl. Sci. Engrg. 5 (1995), 1701–1711.
- [17] C. Sparrow, “The Lorenz equations: bifurcations, chaos, and strange attractors,” Springer-Verlag, New York, 1982.
- [18] Y.-C. Wong, *Differential geometry of grassmann manifolds*, Proc. N. A. S. 57 (1967), 589–594.

Received June 2002; in revised March 2003.

*E-mail address:* [hagen@nethere.com](mailto:hagen@nethere.com)